NOLTR 71-139

FINITE AMPLITUDE PROPAGATION OF AN UNDERWATER EXPLOSION SHOCK WAVE ALONG A STRONGLY REFRACTED RAY TUBE

By
John F. Goertner

1 DECEMBER 1971

NOL

NAVAL ORDNANCE LABORATORY, WHITE OAK, SILVER SPRING, MARYLAND

NOLTR 71-139

UNCLASSIFIED
Security Classification

DOCUMENT CONTROL DATA - R & D

Security classification of title, body of abstract and indexing annotation must be entered when the overall report is classified)

1. ORIGINATING ACTIVITY (*Corporate author*) Naval Ordnance Laboratory White Oak, Silver Spring, Maryland 20910	2a. REPORT SECURITY CLASSIFICATION UNCLASSIFIED 2b. GROUP

3. REPORT TITLE

Finite Amplitude Propagation of an Underwater Explosion Shock Wave Along a Strongly Refracted Ray Tube

4. DESCRIPTIVE NOTES (*Type of report and inclusive dates*)

5. AUTHOR(S) (*First name, middle initial, last name*)

John F. Goertner

6. REPORT DATE 1 December 1971	7a. TOTAL NO. OF PAGES iii + 24	7b. NO. OF REFS 4
8a. CONTRACT OR GRANT NO. b. PROJECT NO DNA Subtask NA 002/20 c. d.	9a. ORIGINATOR'S REPORT NUMBER(S) NOL TR 71-139 9b. OTHER REPORT NO(S) (*Any other numbers that may be assigned this report*)	

10. DISTRIBUTION STATEMENT

Approved for Public Release; Distribution Unlimited

11. SUPPLEMENTARY NOTES	12. SPONSORING MILITARY ACTIVITY Defense Nuclear Agency Washington, D.C.

13. ABSTRACT

The effect of wave overtaking on the peak pressure of refracted underwater explosion shock waves is estimated by means of a finite amplitude calculation for the wave propagation along refracted ray tubes given by simple ray theory. The results indicate that a reduction in peak pressure occurs due to increased wave-overtaking along refracted ray paths to first caustics. Reductions in the peak pressure no greater than 5% occurred for the particular refractive conditions treated, but preliminary work with other conditions indicates much greater reductions can occur.

DD FORM 1 NOV 65 1473 (PAGE 1)

S/N 0101-807-6801

UNCLASSIFIED
Security Classification

14 KEY WORDS	LINK A		LINK B		LINK C	
	ROLE	WT	ROLE	WT	ROLE	WT
Underwater Explosions						
Refraction						
Shock Wave						
Finite Amplitude Wave Propagation						
Caustics						
Nuclear Explosions						
Ray Tracing						

FINITE AMPLITUDE PROPAGATION OF AN UNDERWATER EXPLOSION SHOCK WAVE ALONG A STRONGLY REFRACTED RAY TUBE

Prepared by:
John F. Goertner

ABSTRACT: The effect of wave overtaking on the peak pressure of refracted underwater explosion shock waves is estimated by means of a finite amplitude calculation for the wave propagation along refracted ray tubes given by simple ray theory. The results indicate that a reduction in peak pressure occurs due to increased wave-overtaking along refracted ray paths to first caustics. Reductions in the peak pressure no greater than 5% occurred for the particular refractive conditions treated, but preliminary work with other conditions indicates much greater reductions can occur.

UNDERWATER EXPLOSIONS DIVISION
EXPLOSIONS RESEARCH DEPARTMENT
NAVAL ORDNANCE LABORATORY
WHITE OAK, MARYLAND

NOLTR 71-139 1 December 1971

Finite Amplitude Propagation of an Underwater Explosion Shock Wave Along a Strongly Refracted Ray Tube

Present understanding of the refraction of underwater explosion shock waves has been achieved largely through the use of acoustic theory, i.e., theory of low amplitude pressure waves, with an overall modification to account for explosion pulse propagation. The work reported here is the first part of a study undertaken to determine whether it is necessary to modify the present methods so as to intrinsically incorporate the non-linear effects due to the finite amplitude of explosion pulses. The work was supported by Defense Atomic Support Agency (now Defense Nuclear Agency) Subtask NA 002/20, Underwater Shock Theory/Energy Focusing and Refraction Effects.

The author is indebted to Robert M. Barash for many valuable suggestions during the course of this work.

ROBERT D. WILLIAMSON, II
Captain, USN
Commander

C. J. ARONSON
By direction

CONTENTS

ILLUSTRATIONS

TABLE

LIST OF SYMBOLS

t	Time
x	Distance from charge along ray tube axis
x_o	Starting distance for computation (corresponds to p_{max} = 10,000 psi)
u	Water particle velocity
ϱ	Water density
c	Local sound speed
ϱ_o, c_o	Ambient values of density and sound speed
p	Pressure (relative to ambient water pressure)
p_{max}	Initial pressure at shock front
$(p_{max})_{ISO}$	p_{max} for a spherical shock wave which has traveled the same distance as the refracted one, i.e., in isovelocity water having c_o and ρ_o the same as at the charge location
n	Exponent in modified Tait Equation (taken as 6.0)
σ	Riemann function, $\int_o^p \frac{1}{\rho c}\, dp$
S	Shock velocity
u_s, σ_s	Particle velocity and Riemann function at the shock front
A, $A(x)$	Area of ray tube cross-section
$\ln A$	Natural logarithm of $A(x)$
$A_o(x)$	Cross-sectional area of an equivalent non-refracted ray tube (identical initial boundary rays) at distance, x, from the charge
F	Acoustic wave amplitude factor $= \left[\frac{A_o(x)}{A(x)}\right]^{\frac{1}{2}}$
γ_i	Angle measured at source used to identify refracted ray or ray tube (measured downward from horizontal)

1. INTRODUCTION

A general mathematical solution--either analytic or numerical--to the problem of refraction of an underwater explosion shock wave by a strong velocity gradient does not yet exist. Today's solutions consist of judicious patching together of various asymptotic solutions and experimental results. For example, Brockhurst, Bruce, and Arons (1961)* demonstrated the usefulness of acoustic ray theory in describing refracted wave pressures where strong focusing has not occurred. Near regions of strong focusing in the ocean (convergence zone caustics), Blatstein (1971) has demonstrated the usefulness of a modified wave-length-dependent ray theory to describe the experimentally measured pressure signatures. However, neither simple ray theory nor the modified ray theory take into account the wave overtaking effects inherent to shock wave propagation.** The above mentioned authors in applying their respective treatments incorporated the judicious assumption that the effects of wave overtaking are the same as for a non-refracted underwater explosion shock wave that has traveled the same distance. The purpose of this note is to check this assumption by calculating the propagation of an underwater explosion shock wave along typical acoustically refracted ray tubes. To do this we use a method-of-characteristics numerical integration of the fluid dynamical equations expressing conservation of mass and of momentum in the direction of the ray tube.

This paper consists of three sections. The first describes the approximate theory and lists the pertinent equations. The second gives a brief account of the essential features of the numerical calculations. And, the third summarizes the results calculated for a sampling of refracted ray tubes for a source depth and velocity profile yielding a thermocline-related caustic.

2. THEORY

The problem considered is the inviscid unsteady compressible flow along the axis of a rigid tube of arbitrarily changing area.

Constitutive Equations. The equations used to describe the motion are the momentum and continuity equations and a pressure-density relation for the water.

---

*Refer to list of references on Page 24

**For discussion of wave-overtaking in underwater explosion shock wave propagation see Snay, 1966, Section IV or Cole, 1948, Sections 2.1-2.6

Along the axis of the ray tube the momentum equation reduces to

$$\frac{\partial u}{\partial t} + u \frac{\partial u}{\partial x} + \frac{1}{\rho} \frac{\partial p}{\partial x} = 0 \qquad (1)$$

and the continuity equation becomes

$$\frac{\partial \rho}{\partial t} + u \frac{\partial \rho}{\partial x} + \rho \left(\frac{\partial u}{\partial x} + \frac{u}{A} \frac{\partial A}{\partial x}\right) = 0 \qquad (2)$$

where

t = time
x = distance along the axis
u = particle velocity
p = pressure (relative to the ambient value)
ρ = water density
A = A(x), area of the ray tube cross-section

For the pressure-density relation we used the modified Tait equation (Cole, 1948, page 44).

$$p = \frac{\rho_o c_o^2}{n} \left[\left(\frac{\rho}{\rho_o} \right)^n - 1 \right] \qquad (3)$$

where c_o = ambient sound speed
(subscript "o" indicates ambient state)
n = constant

With n=6.0 equation (3) describes the mechanical behavior of the water behind both shocks and isentropes to within about ± 0.5% for pressures in the range, 0≤p≤10,000 psi; i.e., flow parameters such as the density, sound speed, particle velocity, shock velocity, and Riemann function are estimated to be within about ±0.5% of their true values.*

Essentially, by introducing equation (3) to describe the entire flow, we are neglecting the effects of the small but variable entropy increases which occur as the water is traversed by the outwardly propagating shock front. In this report we will consistently make use of the simplifications which follow from this assumption of uniform entropy throughout the entire flow. As pointed out above, this leads to estimated errors of the order of ±0.5% in the computed flow parameters.

Characteristic Equations. Introducing the Riemann function

$$\sigma = \int_o^p \frac{1}{\rho c} \, dp \qquad (4)$$

*These accuracy limits were estimated from Tables 3.3 and 3.4 of NOLTR 70-31 (H. G. Snay and A. R. Kriebel, 1970) By making use of "Zeta equation" as an intermediate standard. Using n=6.0, equation (3) is essentially equivalent to the Zeta equation; and, over the pressure range, zero to 10,000 psi, the calculated values behind shocks and isentropes for all the mechanical flow parameters are the same to within ±0.2%.

and noting that

$$c^2 = \frac{dp}{d\rho} \tag{5}$$

equations 1 and 2 can be transformed to

$$\frac{\partial(u+\sigma)}{\partial t} + (u+c)\frac{\partial(u+\sigma)}{\partial x} = -\frac{uc}{A}\frac{\partial A}{\partial x} \tag{6}$$

$$\frac{\partial(u-\sigma)}{\partial t} + (u-c)\frac{\partial(u-\sigma)}{\partial x} = +\frac{uc}{A}\frac{\partial A}{\partial x} \tag{7}$$

In deriving equations (6) and (7) we have implicity used the uniform entropy assumption.*

Equations (6) and (7) are the so-called "characteristic equations." They give the time rates of change of the quantities $(u+\sigma)$ and $(u-\sigma)$ to observers traveling in the x-t plane at velocities $(u+c)$ and $(u-c)$, respectively. Given suitable boundary conditions they can be integrated numerically throughout the region in the x-t plane between the outward-propagating shock front and some starting point (value of x) along the ray tube.

To solve equations (6) and (7) and also to calculate the pressure we need several additional relations. The following are derived from equations (3), (4), and (5):

Sound speed $$\frac{c}{c_o} = \left(\frac{\rho}{\rho_o}\right)^{\frac{n-1}{2}} \tag{8}$$

Pressure $$p = \frac{\rho_o c_o^2}{n}\left[\left(\frac{c}{c_o}\right)^{\frac{2n}{n-1}} - 1\right] \tag{9}$$

Riemann function $$\sigma = \frac{2}{n-1}\left(c-c_o\right) \tag{10}$$

Shock front boundary condition $$u_s - \sigma_s = 0 \tag{11}$$

Shock front velocity $$\frac{s}{c_o} = 1 + \frac{n+1}{4}\frac{u}{c_o} \tag{12}$$

*For elucidation of the role of entropy and the significance of the Riemann function, the reader is referred to NOLTR 65-52, H. G. Snay, 1966, pages 46-50.

Equation (11) follows from (7) neglecting the entropy change across the shock. Equation (12) is derived from the mechanical shock relation, $p=\rho_o uS$, (conservation of mass and momentum) using equations (9) and (11) and expanding the term $\left(\frac{c}{c_o}\right)^{\frac{2n}{n-1}}$ in (9) as a function of $\left(\frac{c-c_o}{c_o}\right)$ and dropping terms of 3rd and higher order.

3. NUMERICAL CALCULATIONS

For numerical integration, equations (6) and (7) were approximated by the following difference equations:

$$\Delta^+ (u+\sigma) = -\left[uc \frac{\partial \ln A}{\partial x} \right]_{ave} \Delta t \tag{13}$$

$$\Delta^- (u-\sigma) = +\left[uc \frac{\partial \ln A}{\partial x} \right]_{ave} \Delta t \tag{14}$$

where

Δ^+ = change between mesh points along a positive (u+a) characteristic.
Δ^- = change between mesh points along a negative (u-a) characteristic.

"Average" refers to the end (or mesh) point values. The characteristic mesh is approximated by line segments of slope $(u+c)_{ave}$ and $(u-c)_{ave}$.

For a more complete description of the method of computation, the reader is referred to Goertner, 1965, Appendix B. In this section we will discuss details which are unique to these computations.

Initial and Boundary Conditions. To start the computation (initial condition) and for the boundary condition at the starting ray tube section we used the shock wave similitude equations derived from experimental data for TNT and Pentolite (Cole, 1948, pages 238-242):

$$p_{max} = k \left(W^{1/3}/R \right)^{1.13} \tag{15}$$

$$\theta/W^{1/3} = 0.060 \left(W^{1/3}/R \right)^{-0.18} \tag{16}$$

where

p_{max} = initial shock pressure in pounds per square inch
W = weight of TNT in pounds
R = range in feet
θ = time constant of the exponential pressure pulse in milliseconds.

$k = 2.16 \times 10^6$ for TNT
$= 2.25 \times 10^6$ for Pentolite

Figure 1 illustrates how this was done. Using equation (15), the range corresponding to p_{max}=10,000 psi is calculated. In the figure, x_o is the starting point for the computation; this is set equal to the range corresponding to p_{max}= 10,000 psi. At $x=x_o$ the pressure, and from this, the Riemann function, is calculated using the time constant, θ, given by equation (16). This is the boundary condition used at $x=x_o$.

To start the computation, N suitably spaced mesh points are placed along the shock path through the point (x_o, 0) corresponding to the similarity equation (15). For these computations, the N initial mesh points were inserted along the shock in the interval from $x = x_o$ to $1.1\, x_o$. For simplicity, the sketch illustrates only 4 initial mesh points; generally a greater number - 32, 64, or 128 - were required. Using equations (9) through (12) we can calculate the shock path and all pertinent flow variables along the "starting shock." Starting at the first inserted mesh point, the numerical integration then proceeds from shock front to $x=x_o$ along successive negative characteristics.

Convergence of the Numerical Computations. In the course of development and check-out, three versions of the computer program were used. The essential difference among these was in how the term $\left[uc \frac{\partial \ln A}{\partial x} \right]_{ave}$ in equations (13) and (14) was computed (approximated) and in the degree of control over this approximation.

Version 1 was specifically written to calculate the shock wave propagation along a spherically diverging ray (i.e., a cone). For this case $\partial \ln A/\partial x = 2/x$ so that in solving equations (13) and (14) the term in brackets could be evaluated at the appropriate mesh points and then averaged.

Version 2 was written for the ray tube of arbitrarily changing area; A(x) being calculated by 3-point Lagrangian interpolation of tabulated values. This led to a slightly different approximation, namely,

$$\left[uc \frac{\partial \ln A}{\partial x} \right]_{ave} = \frac{\overline{(uc)}}{\overline{A}} \frac{\Delta A}{\Delta x} \qquad (17)$$

where the "bar" indicates average and "Δ" the difference of the appropriate mesh point values.

The result of these different representations of $\left[uc \frac{\partial \ln A}{\partial x} \right]_{ave}$ in equations (13) and (14) on the shock front pressure calculated for a spherically spreading shock is shown in Figure 2. We see that as N increases the pressure-vs-distance curves

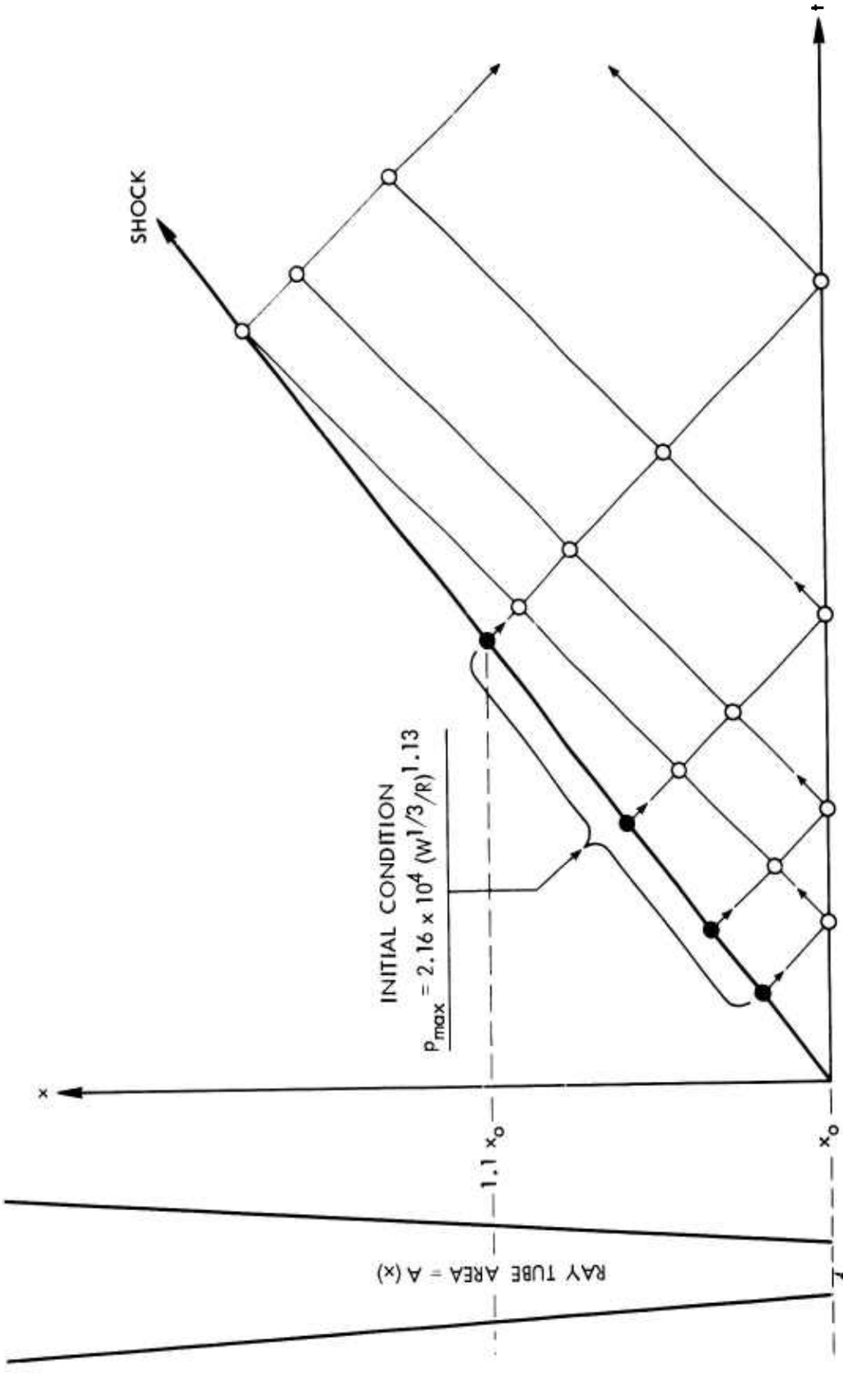

FIG. 1 SKETCH ILLUSTRATING GEOMETRY OF COMPUTATION

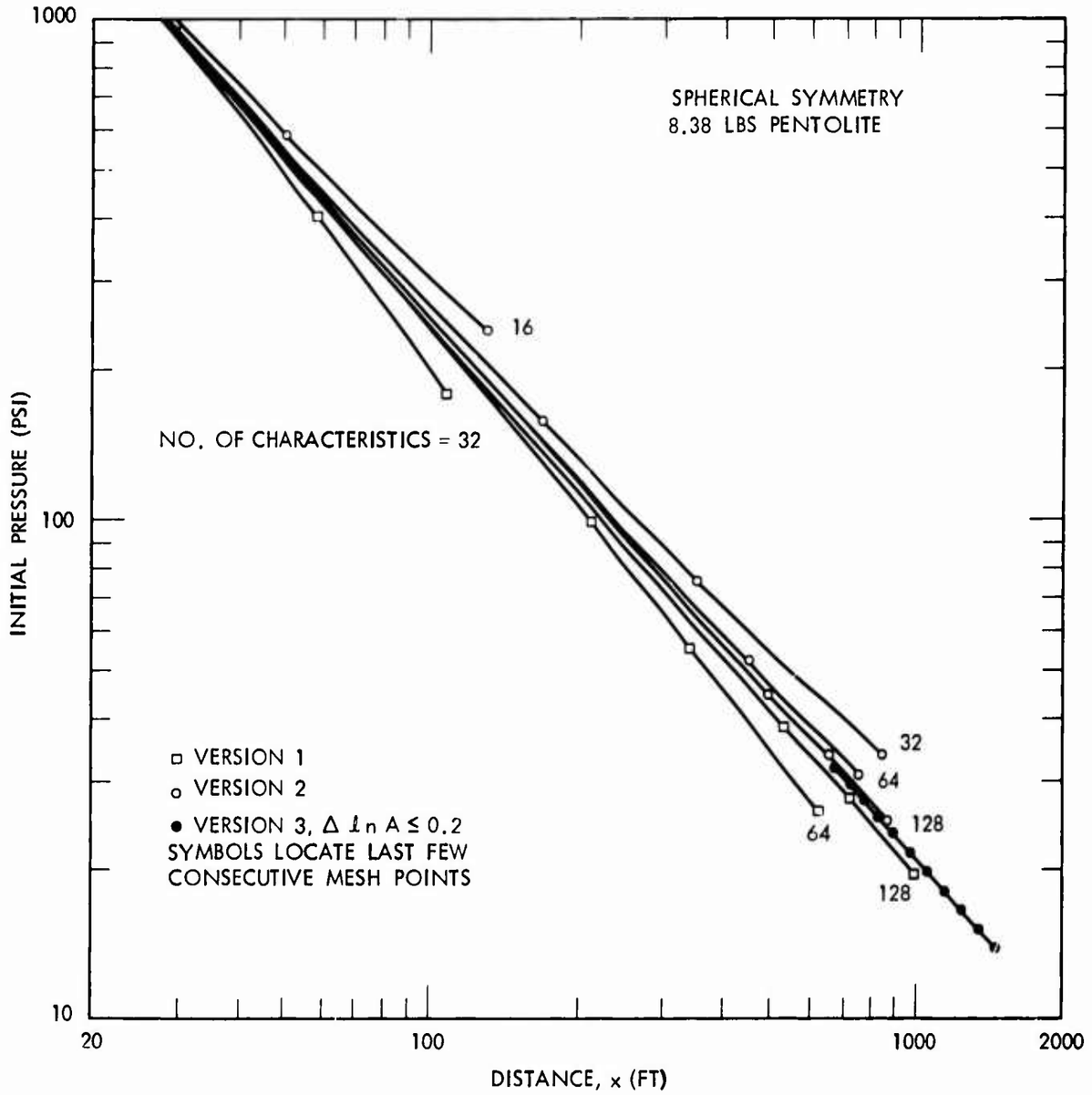

FIG. 2 VARIATION OF CALCULATED PRESSURE-DISTANCE WITH MESH SIZE

calculated using these different approximations converge from opposite sides to what is apparently the true solution to equations (6) and (7). Thus, by good fortune, we obtained a valuable check on the computations.

Control of the Divergence Term. As the computation proceeds the shock front moves outward and the separation of adjacent mesh points increases (Figure 1). As a result, the approximation to $uc\frac{\partial \ln A}{\partial A}$ computed from parameters at the adjacent mesh points becomes poorer and the numerical solution degenerates as can be seen in Figure 2. Our initial solution to this problem was simply to increase--double, re-double, etc.--N, the number of initial negative characteristics, until the numerical solution had apparently converged. This worked--except for some ray tubes which diverged rapidly upon entering a partial shadow zone. For these the rate of convergence with increasing N was too slow and computer cost became excessive.

To compute along these rays we designed Version 3 which subdivided the characteristic net--introduced additional characteristics and discarded others--as the computation proceeded. The modifications which constitute Version 3 stem from the following observations:

(1) That the computation time is roughly proportional to the number of mesh points calculated.

(2) That in both Versions 1 and 2 the major source of systematic computational error appears to be the finite difference approximation to $\partial \ln A/\partial x$ (Equations 13 and 14).

Thus, in Version 3 we attempted to calculate the minimum number of mesh points consistent with some preassigned level of overall computation error. We did this by monitoring $\Delta \ln A$ from point to point along the shock trajectory. In the event

$$\left| \Delta \ln A \right| > \left[\Delta \ln A \right]_{max} \tag{18}$$

where $\left[\Delta \ln A\right]_{max}$ is some preset value, the computation switched to a subroutine which introduced N/2 intermediate mesh points along the half of the previous negative characteristic adjacent to the shock, discarded the N/2 mesh points from the other half, did the necessary bookkeeping, and then returned to re-calculate the next point on the shock trajectory. If necessary, this procedure was repeated until

$$\left| \Delta \ln A \right| \leq \left[\Delta \ln A \right]_{max} \tag{19}$$

Figure 2 includes a segment of a pressure-vs-distance curve calculated using Version 3 with $\left[\Delta \ln A\right]_{max}$ set equal to 0.2; it falls between the curves calculated using Versions 1 and 2. With Version 3 the shock trajectory is essentially independent of N, the number of initial characteristics. (Using this program, the value specified for N essentially determines the area of integration in the x-t plane, and is generally specified in accordance with the required p-t signature duration at some value of x.)

The value, $\left[\Delta \ln A\right]_{max}=0.2$, was selected for the ray tube computations summarized in Part 4. This value was selected by inspection of the calculated pressure-vs-distance data such as shown in Figure 3 and Table 1.

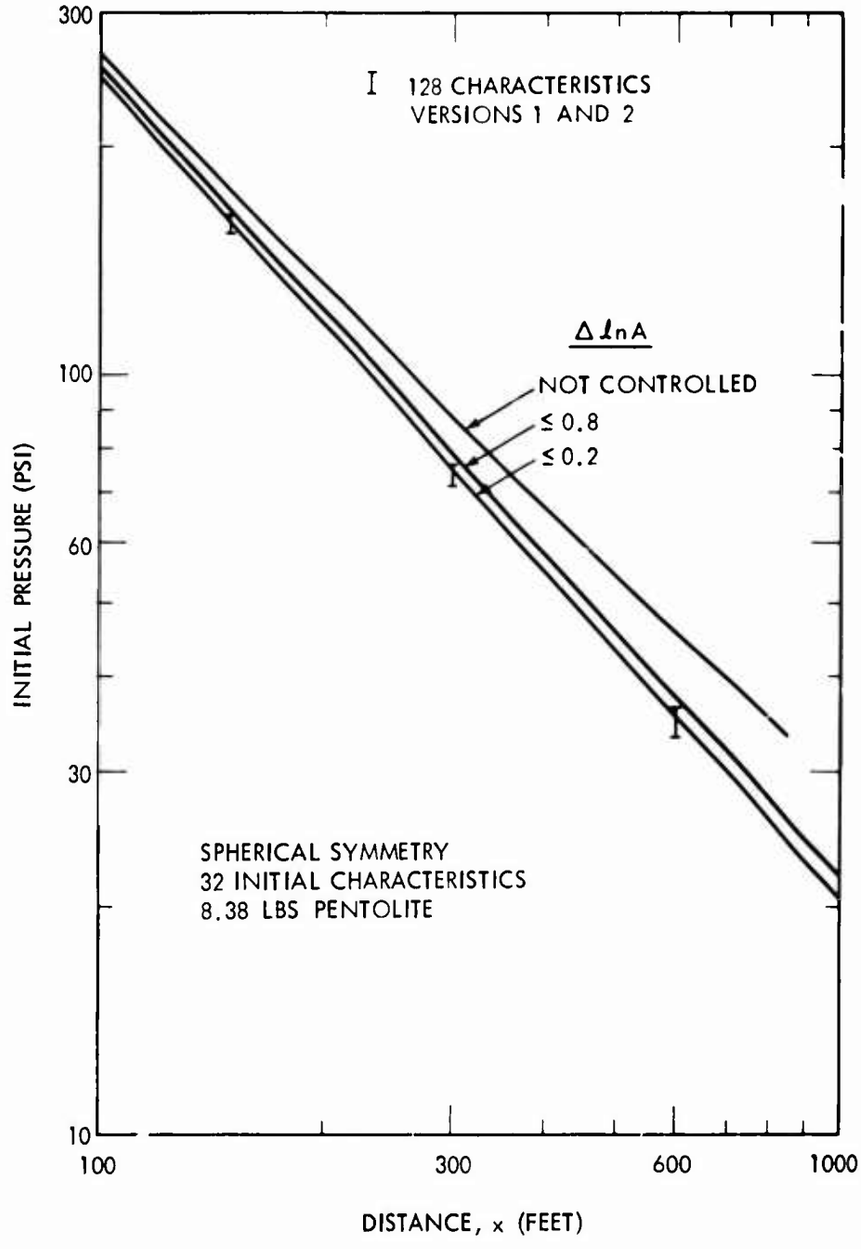

FIG. 3 VARIATION OF CALCULATED PRESSURE-DISTANCE WITH REZONING

TABLE 1

CHANGE IN CALCULATED SHOCK FRONT PRESSURE, p_{max}, AS A FUNCTION OF $\left[\Delta \ln A\right]_{max}$

$x = 200$ ft ($p_{max} = 216$ psi)

8.38 lbs pentolite
32 initial characteristics
spherical symmetry

$\left[\Delta \ln A\right]_{max}$	Relative Error in p_{max} (%)
0.1*	——
0.2	+0.3
0.4	+1.5
0.8	+4.6
(Not Controlled)	+13.6

*For this case 64 initial characteristics were required in order to compute out to x = 200 feet.

4. RESULTS FOR REFRACTED RAY TUBES

We started this study by looking at refracted rays corresponding to the flooded quarry experiment of Brockhurst, Bruce, and Arons (1961). Figure 4 shows the measured average sound velocity profile and the corresponding ray diagram computed by ray theory. The locations of the rays used are indicated by the symbols, "A" through "E."

For each of these chosen rays we also calculated the trajectories of two adjacent rays which defined the ray tube for our calculations. Figures 5 through 9 show the ray tube areas for these rays as a function of distance along the central ray; and, compares this with the corresponding area for a non-refracted ray tube. Note that in Figures 5 through 9 it is the logarithms of the ray tube areas and path lengths which are plotted. This is appropriate since it is the rate of change of lnA (equations 13 and 14) which governs the wave propagation along the tube; and, it is the ratio, $R/W^{1/3}$, which enters into the boundary and initial conditions of the calculation (equations 15 and 16). This is also in accordance with the principle of similarity for underwater explosion shock waves (Cole, 1948, page 110) which holds for spherical waves but <u>not</u> for waves propagating along refracted ray tubes (since each refracted ray tube has a characteristic length of its own which is independent of the charge size).

We now make use of the shock wave similarity principle for spherical waves to compare the ray tube area functions of Figures 5 through 9. We do this by superposing the plots, Figures 5 through 9, and sliding them along the straight line representing the spherical wave until we have aligned the points of departure from spherical spreading. (Note, if two area functions can be made to coincide in this manner, then they are similar in the sense that a calculation for one can be scaled to the other--corresponding values of $W^{1/3}$, path lengths, and times will be in the ratio of the path lengths for corresponding points of the area functions). The result of such a superposition of the area functions is shown in Figure 10, which, for the purpose of this report, shows the essential differences among these functions.

Our selection of area functions (Figure 10) is characterized by two extremes, case "B" where the tube cross-section goes rapidly to zero as the ray approaches the caustic, and ray "C" where the tube cross-section undergoes rapid expansion as it enters the shadow zone behind the caustic.

RAY TUBE APPROACHING CAUSTIC

Results for wave front pressures, p_{max}, calculated along a ray tube approaching the caustic are shown in Figure 11. These results are presented in terms of the amplitude factor,

$$F \equiv \left[\frac{A_o(x)}{A(x)}\right]^{\frac{1}{2}} \tag{20}$$

where $A(x)$ = ray tube cross-sectional area at distance, x, along the central ray

$A_o(x)$ = ray tube cross-sectional area of an equivalent non-refracted ray tube (identical initial boundary rays) at distance, x, from the charge, i.e., in this case the area of the zone of a sphere of radius, x, cut by the boundary rays.

(Text continued on page 20)

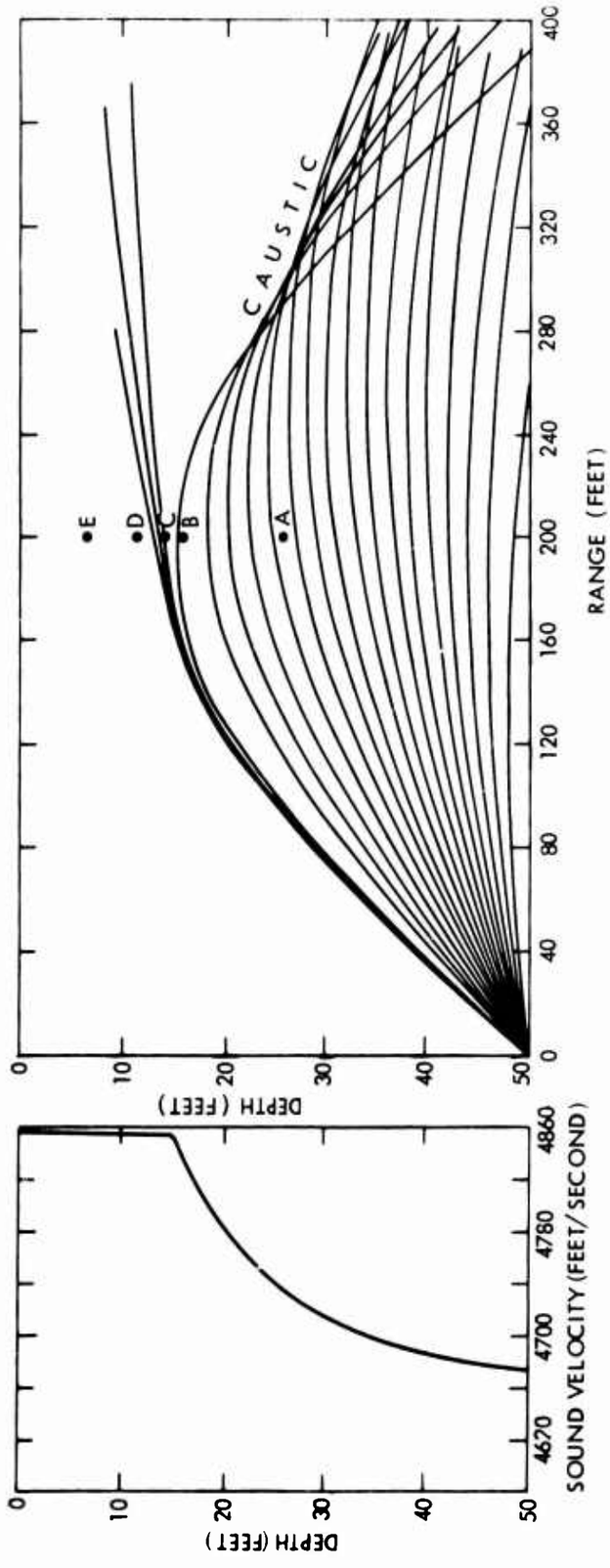

FIG. 4 VELOCITY PROFILE AND RAY DIAGRAM SHOWING LOCATION OF RAY TUBES SELECTED FOR CALCULATIONS

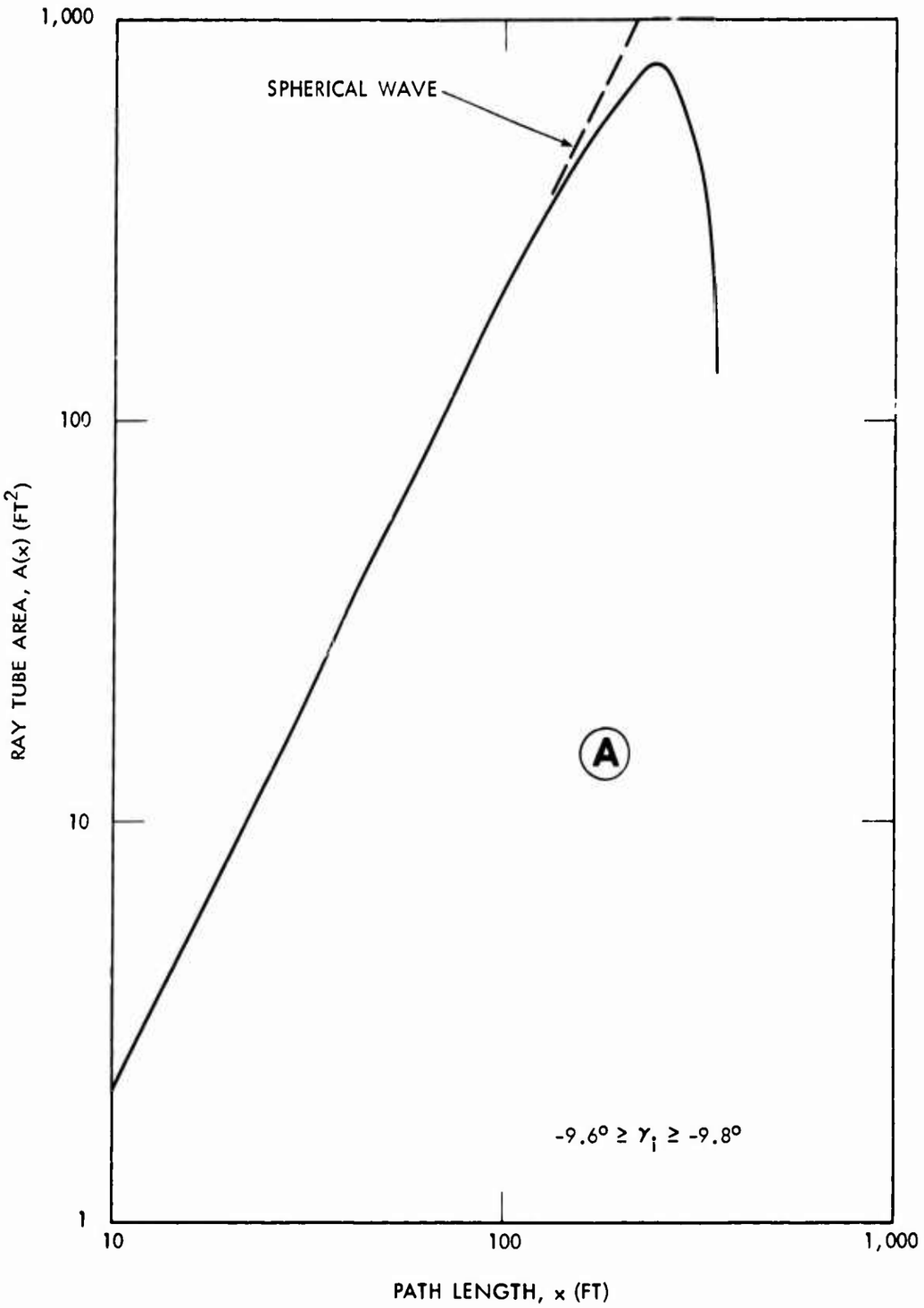

FIG. 5 RAY TUBE AREA AS A FUNCTION OF PATH LENGTH -- $\gamma_i = -9.7^{\circ}$

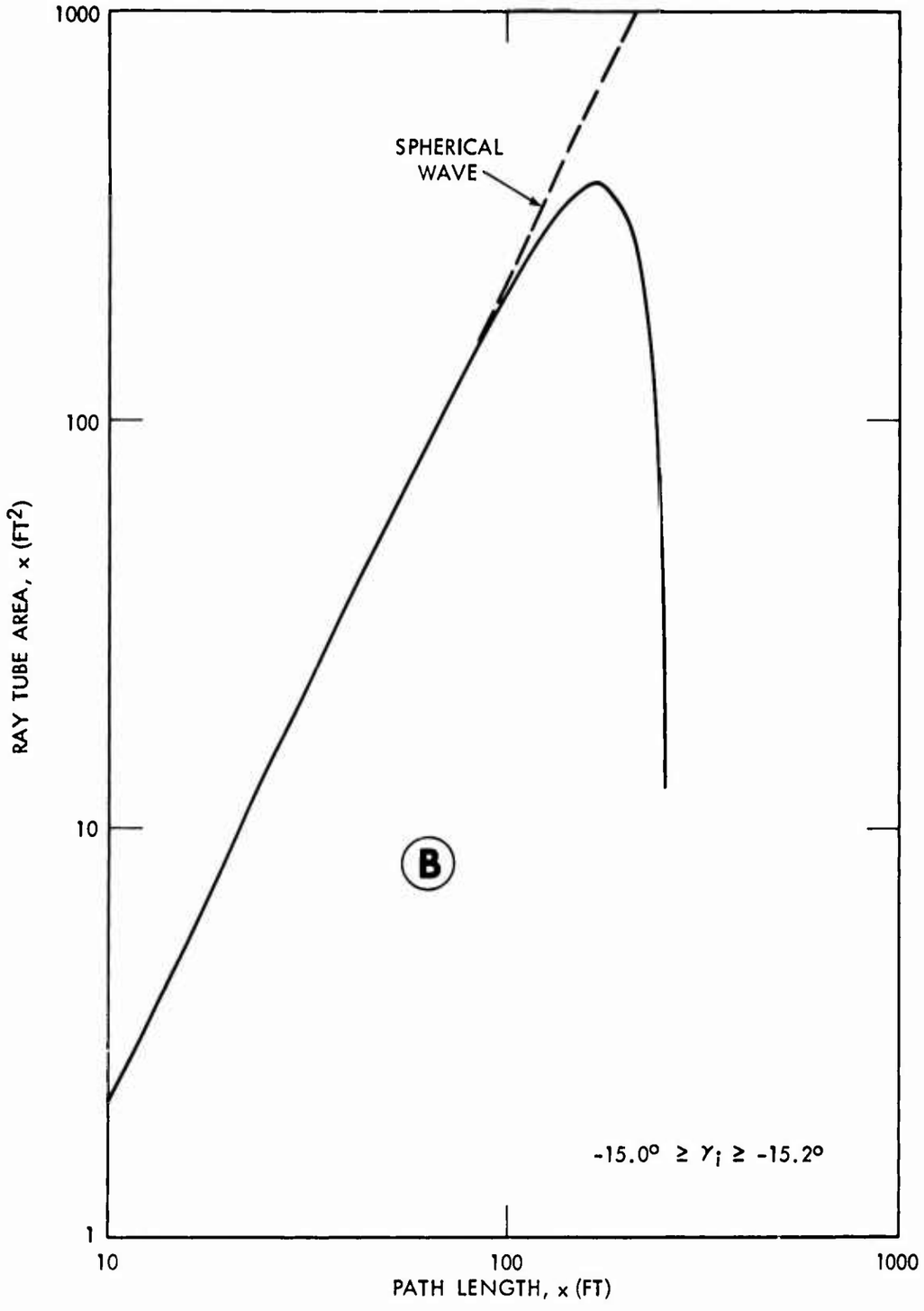

FIG. 6 RAY TUBE AREA AS A FUNCTION OF PATH LENGTH -- $\gamma_i = -15.1°$

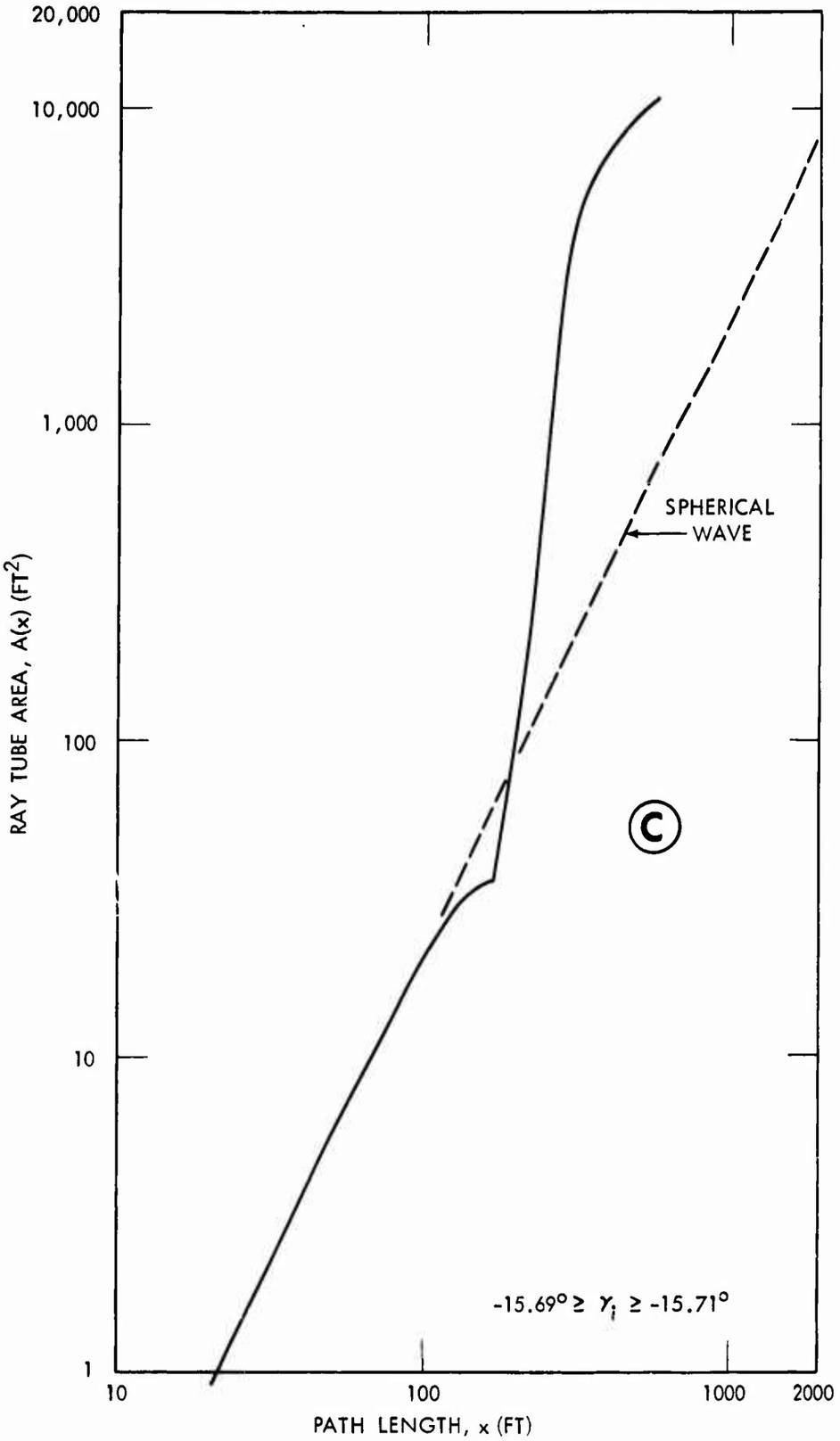

FIG. 7 RAY TUBE AREA AS A FUNCTION OF PATH LENGTH -- γ_i = -15.7°

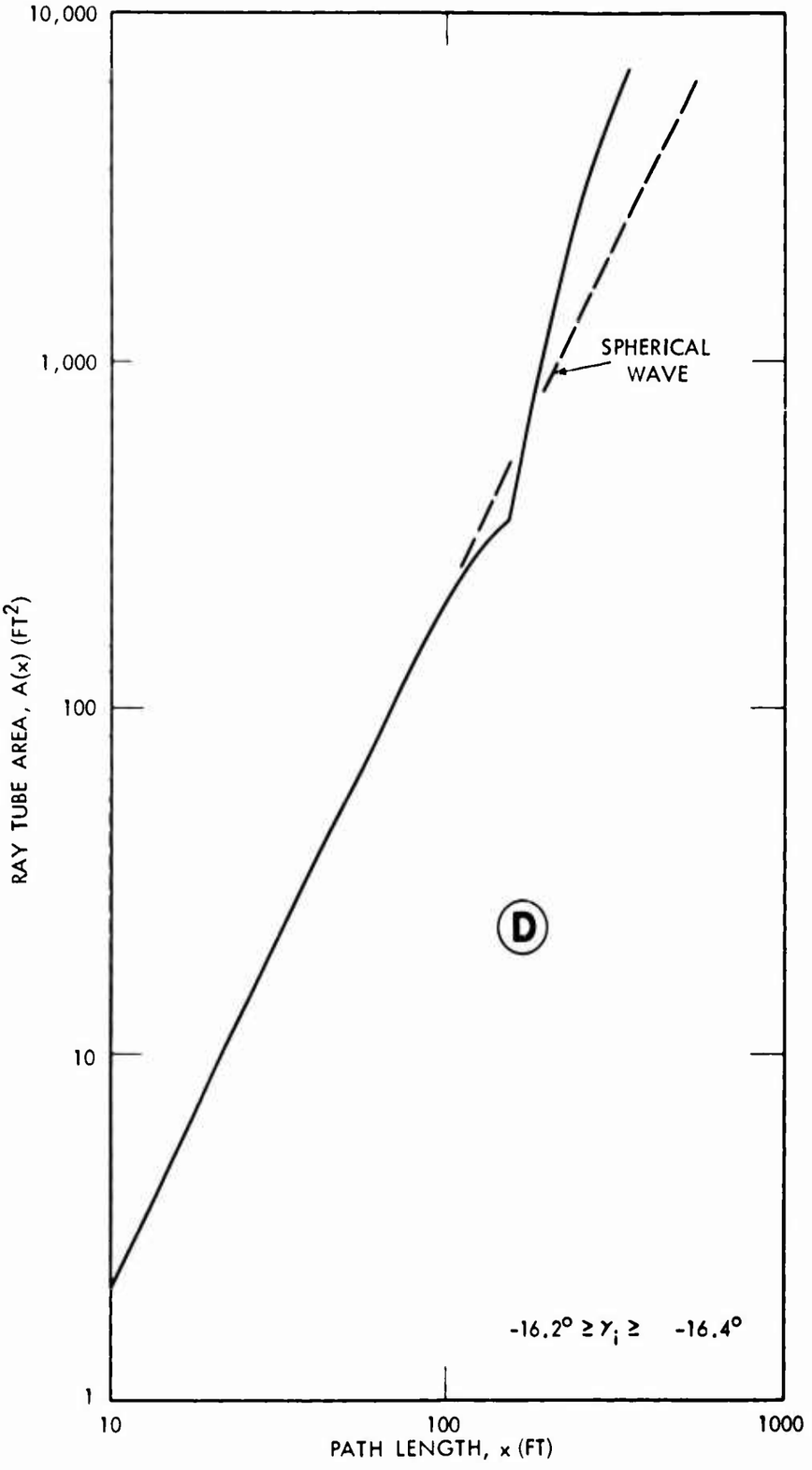

FIG. 8 RAY TUBE AREA AS A FUNCTION OF PATH LENGTH -- $\gamma_i = -16.3°$

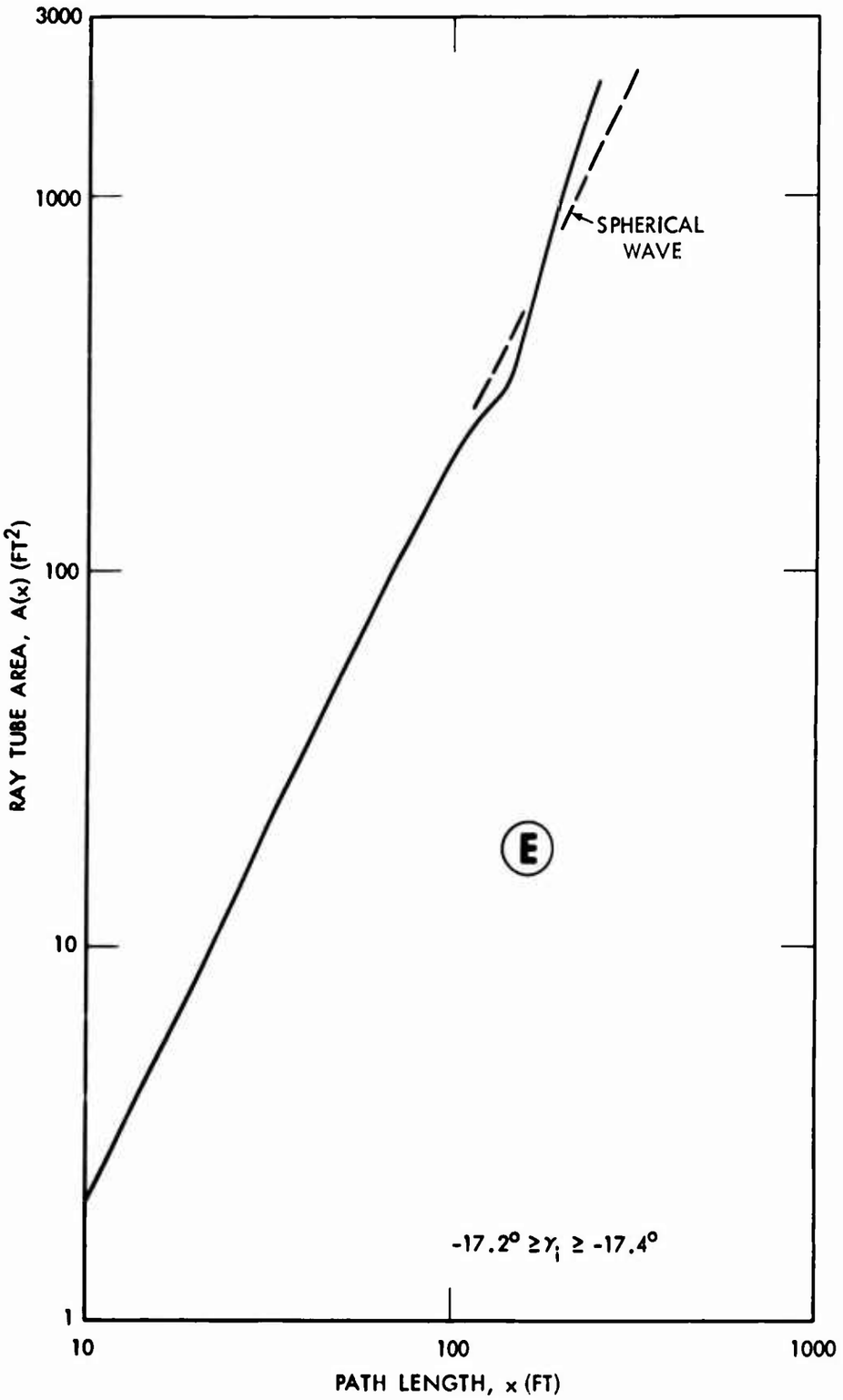

FIG. 9 RAY TUBE AREA AS A FUNCTION OF PATH LENGTH -- $\gamma_i = -17.3°$

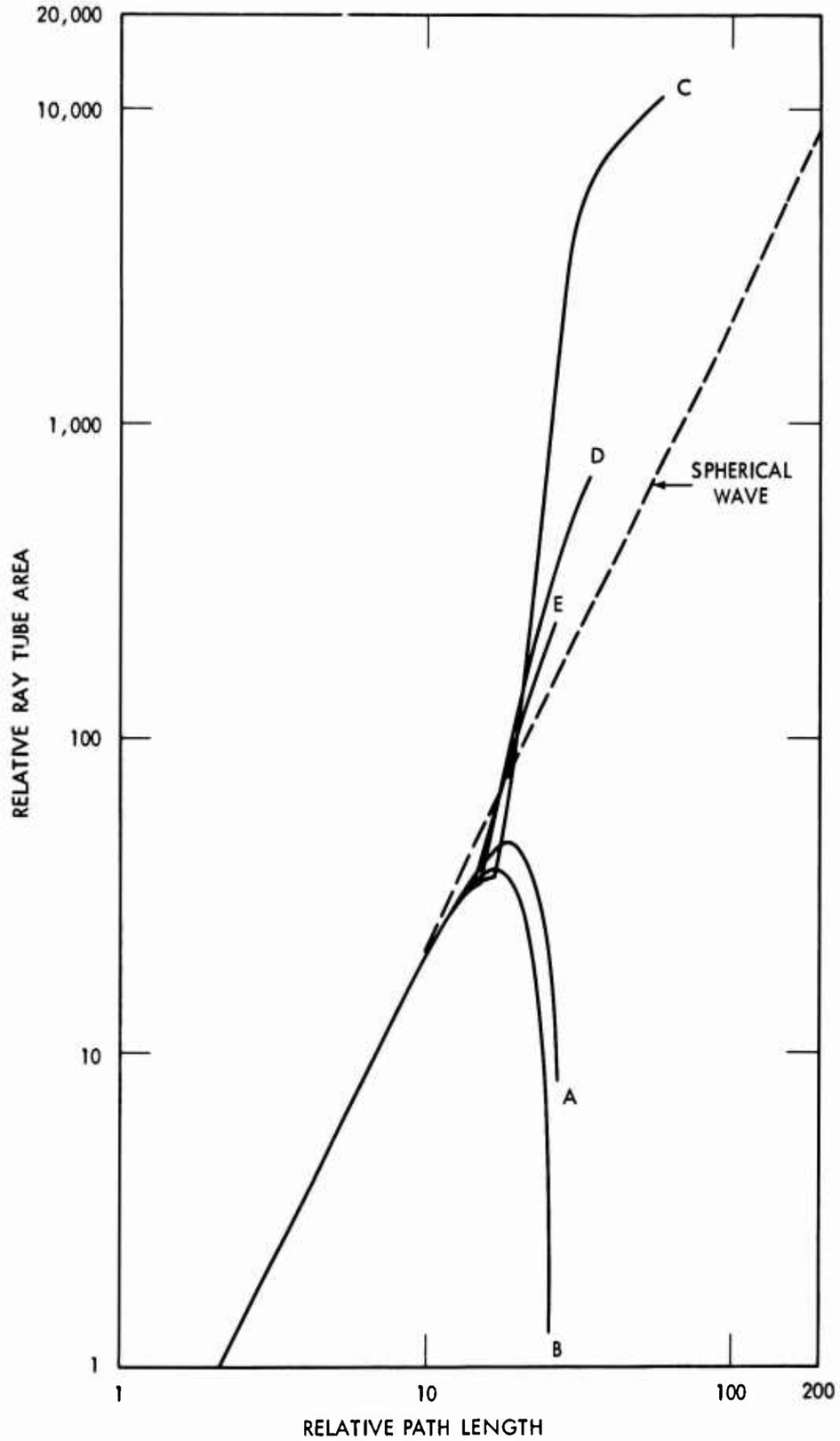

FIG. 10 COMPARISON OF RAY TUBE AREA FUNCTIONS

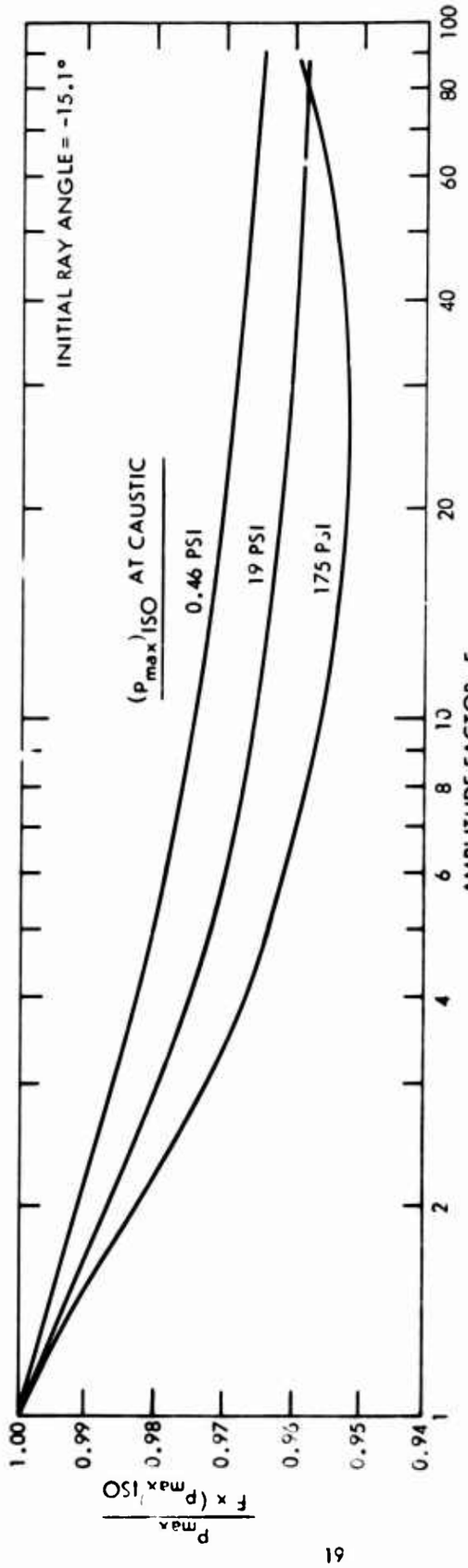

FIG. 11 EFFECT OF WAVE-OVERTAKING ON p_{max} AS SHOCK WAVE APPROACHES A CAUSTIC

The product

$$F \times (p_{max})_{ISO}$$

is then the amplified pressure which would occur along the ray tube if there were no wave overtaking, i.e., in the acoustic approximation--$c = c_o$ = constant. The ratio,

$$\frac{p_{max}}{F \times (p_{max})_{ISO}}$$

therefore, expresses the reduction in p_{max} due to wave overtaking caused by convergence of the ray tube as it approaches the caustic.

Since we are interested in isolating the effects due to wave-overtaking, both the refracted and isovelocity signatures were taken from calculations which are identical except for the cross-sectional area functions. Thus, in the comparison, small errors introduced through the approximate pressure-density relation (equation 3) and the shock wave similtude equations (15) and (16) are essentially cancelled.

The curves shown in Figure 11 were calculated for the ray, $\gamma_i = -15.1^o$ (case B), but when presented in this manner are identical to those for the ray, $\gamma_i = -9.7^o$ (case A). The three curves presented in Figure 11 were calculated for three different TNT charge weights--56, 0.115, and 2.6×10^{-6} lbs--which yield spherical wave pressures (no refraction), p_{max}=175, 19, and 0.46 psi, at 256 ft from the charge, the path length along this particular ray to the caustic. The 0.115 and 2.6×10^{-6} lb TNT charge weights were chosen to scale the caustic location (x=256 ft for this quarry profile) to x=180,000 ft for 20 kiloton and 900 lb TNT charges, respectively. The scaled caustic location and the 900-lb charge weight correspond to the Sargasso Sea experiment (Blatstein, 1971).

In the ocean experiment, the caustic was a convergence zone caustic. When we did these calculations we had hoped that the results would be approximately correct for rays en route to convergence zone caustics in the ocean as well as to thermocline-related caustics. But, subsequent calculations using ray tubes to convergence zone caustics show that the results presented in Figure 11 are not even approximately correct for convergence zone ray tubes--for these, the reduction in p_{max} due to wave-overtaking as the shock wave travels to the caustic is generally much greater, sometimes amounting to a reduction p_{max} of 25 or 30%. We also point out that the results presented in this section are based on a single experimentally measured sound velocity profile. Thus, the results presented in Figure 11 may, or may not, be typical of explosion geometries which form thermocline-related caustics.

Note that to use Figure 11 we must have additional knowledge as to the refractive effects at the caustic. In practice the amplitude factor, F, computed from the ray tube area of a ray theory computation is of no use in estimating the effects of wave-overtaking using Figure 11, since in the area of interest wave diffraction has already negated such a computation. Consequently, to use Figure 11

one must resort to experimental data or a modified ray theory computation to obtain a value for F, using the equation

$$F \cong p'_{max}/(p_{max})_{ISO} \tag{21}$$

where p'_{max} is some value of p_{max} from which one can estimate an effective ray tube area and $(p_{max})_{ISO}$ is the pressure of a spherical wave which has traveled the same path length.

In the quarry and ocean experiments to date increases in peak pressure of, say, 4, 6, or 10--but no greater than a factor of 10--have been observed at caustics. This is also true of the results of modified ray theory computations based on sound velocity profiles taken from these experiments. Thus, according to the curves shown in Figure 11 reductions in p_{max} due to wave-overtaking of up to 4 or 5% occur as the shock wave approaches this particular caustic.

RAY TUBE EXPANDING IN SHADOW ZONE

Figure 12 shows the calculated pressure as a function of distance along the ray, $\gamma_i = -15.7^o$ (case C), and compares it with the pressure calculated for a spherically expanding shock wave. For this case the deviation in p_{max} from spherical wave pressure can be predicted quite well by

$$p_{max} = F \times (p_{max})_{ISO} \tag{22}$$

which is also shown in Figure 12 (dashed line). Out to 350 ft equation 22 gives p_{max} to approximately ±1%--at x=600 ft equation 22 predicts a value of p_{max} about 4% lower than computed by the finite amplitude calculation.

5. DISCUSSION AND CONCLUSIONS

As pointed out in the introduction, existing solutions to the refraction problem (ray theory and modified ray theory) do not take into account wave-overtaking and molecular absorption. However, the computed pressures are generally corrected afterwards in the same ratio as the correction for wave-overtaking and absorption estimated for a spherically diverging wave which has traveled the same distance. The purpose of this paper was to check this approximate method of accounting for wave-overtaking. To do this we made an essentially exact calculation including the effects of wave-overtaking (but not absorption) for an approximate problem: namely, the propagation of an underwater explosion shock wave along a duct formed by two adjacent rays calculated by ray theory.

The computational results (Section 4) are for two extreme cases--a converging ray tube approaching a caustic and one undergoing rapid expansion as it enters the shadow region behind the caustic. These were selected from a particular sound velocity profile forming a thermocline-related caustic. For these cases the approximate procedure (estimating the wave-overtaking effects from the spherical wave) introduced a maximum error of ±5%. But, as pointed out in Section 4, this result may or may not be typical of ray tubes to thermocline-related

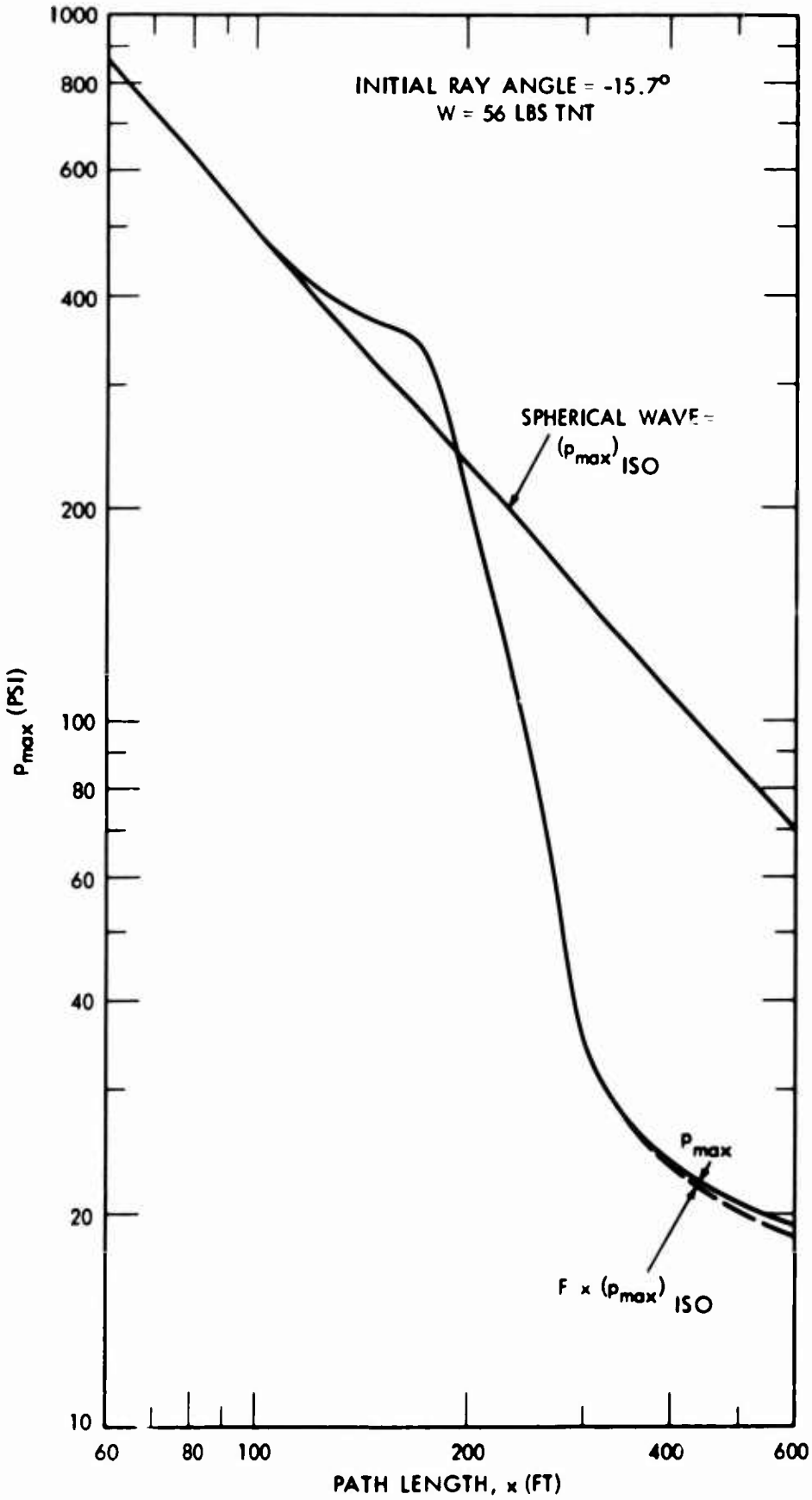

FIG. 12 CALCULATED INITIAL PRESSURE, p_{max}, ALONG AN EXPANDING RAY TUBE

caustics. Also, subsequent calculations covering a range of sound velocity profiles yielding convergence zone caustics resulted in considerably greater reductions in p_{max} due to wave-overtaking. For these cases most of the attenuation ocurred along the portion of the ray path in the deep ocean velocity gradient.

Figure 11 shows that for ray tubes approaching this particular thermocline-related caustic there is increased attenuation of p_{max} due to wave-overtaking as the pressure builds up. This additional attenuation is dependent on the size of the charge--or the pressure level of the wave approaching the caustic--in addition to the variations in ray-tube cross-sectional area between the charge and the caustic. The moderate magnitude of the wave-overtaking corrections to p_{max} would appear to justify the current practice of predicting explosion pressures at and near caustics with modified ray theory computations. Such results can then be adjusted, if necessary, for attenuation due to wave-overtaking occurring along the path to the caustic by the method presented in this report.

Several results from subsequent calculations of wave propagation along ray tubes to convergence zone caustics in the ocean have been mentioned above. Further results and details of these calculations will be given in a subsequent report.

REFERENCES

Blatstein, I. M., 1971, J. Acoust. Soc. Am. 49, 1568-1579

Brockhurst, R. R., Bruce, J. G., and Arons, A. B., 1961, J. Acoust. Soc. Am. 33, 452-456

Cole, R. H., 1948, "Underwater Explosions," Princeton University Press

Goertner, J. F., 1965, "Pressure Waves in the Air Above a Shallow Underwater Explosion: An Approximate Calculation by the Method of Characteristics," NOLTR 65-31